Tellus (2005), 57A, 65–83
Printed in UK. All rights reserved

TELLUS

On the weakening of Hurricane Lili, October 2002

By T. N. KRISHNAMURTI[1]*, J. SANJAY[1]†, T. S. V. VIJAYA KUMAR[1], ADAM J. O'SHAY[1] and RICHARD J. PASCH[2], [1]*Department of Meteorology, Florida State University Tallahassee, FL 32306-4520, USA;* [2]*Tropical Prediction Center, National Hurricane Center, NOAA/NWS, Miami, FL 33165-2149, USA*

(Manuscript received 22 December 2003; in final form 27 May 2004)

ABSTRACT

This paper addresses the weakening of Hurricane Lili of October 2002 just before it made landfall in Louisiana. This hurricane weakened from a category 4 storm on October 3, 2002 at 0000 UTC to a category 1 storm on October 3, 2002 at 1300 UTC. This sudden drop in intensity has been a subject of considerable interest. In this paper we explore a forecast model diagnostic approach that explores the contribution to the hurricane intensity changes arising from a number of dynamical and physical possibilities. Running several versions of a global model at very high resolution, the relative contribution to the intensity drop of Lili arising from cooler sea surface temperatures, dry air advection into the storm, advective non-linear dynamics, non-advective dynamics, and shallow and deep cumulus convection was examined. This line of inquiry led to the conclusion that dry air advection from the north into the storm and the slightly cold sea surface temperatures were not the primary contribution to the observed pressure rise by 22 hPa. The primary contribution to the pressure rise was found to be the 'rest of dynamics' (the non-advective dynamics). The shallow convection contributed slightly to an overall cooling, i.e. a weakening of the warm core of Lili. The effects of deep cumulus convection appeared to be opposite, i.e. towards maintaining a strong storm. A primary term in the 'rest of dynamics', the advection of Earth's angular momentum into the storm, is identified as a major contributor for the intensity change in the analysis. This feature resembles an intrusion of dry air into the core of the storm. This intrusion contributes to a reduction of spin and an overall rapid weakening of the hurricane. The angular momentum partitioning appears quite revealing on the sudden demise of Lili.

1. Introduction

Hurricane Lili made landfall on the west side of Vermillion Bay in Louisiana on October 3, 2002 with category 1 intensity on the Saffir–Simpson Hurricane Scale. This hurricane had strengthened rapidly over the central Gulf of Mexico to category 4 intensity on October 2, 2002. Lili had a well-defined eye during this stage, with dense cloud cover around the eye [Fig. 1a, courtesy of the National Oceanic and Atmospheric Administration (NOAA)]. The banding of clouds over the south-west quadrant of the system was not as prominent as in several other intense hurricanes. Dense high clouds extended north of Lili over the coastal area of Louisiana. A major, unexpected, weakening in the intensity of this hurricane occurred between the night of October 2 and early morning of October 3. Figure 1b (courtesy of Ray Sterner and Steve Babin, Johns Hopkins University) shows a schematic presentation of the track and intensity of Lili from September 21 (when it was first designated as a tropical depression) to October 4 [the time at which the Tropical Prediction Center/National Hurricane Center (TPC/NHC) stopped issuing advisories since it weakened to a depression]. The light blue, green, yellow and orange circles denote the growth stage of Lili from categories 1–4, respectively. Nearly all of the operational forecasts called for a much stronger hurricane at landfall in the United States. Figure 2 illustrates the intensity and track forecasts from several of the current operational models about a day before landfall. As can be seen, the track forecasts were in reasonably good agreement on landfall over the west-central coast of Louisiana, whereas the intensity forecasts, in most cases, predicted an intense hurricane at landfall. 2-d and 3-d forecasts of landfall were quite similar in this regard, and were not very useful for providing operational guidance on the weakening of the hurricane during the last 13 h prior to landfall.

We noted that the forecast errors from a comprehensive physical–dynamical high-resolution global model were generally quite small during the first 6 h of forecasts. This suggested that we could carry out a sequence of 6-h forecasts to explore a subsequent diagnosis of model output to address the question of the weakening of Hurricane Lili. Because the forecast errors are minimum in this sequence of 6-h forecasts, it became possible to perform a partitioning of the model contributions to the intensity

*Corresponding author.
e-mail: tnk@io.met.fsu.edu
†Permanent affiliation: Indian Institute of Tropical Meteorology, Pune 411 008, India.

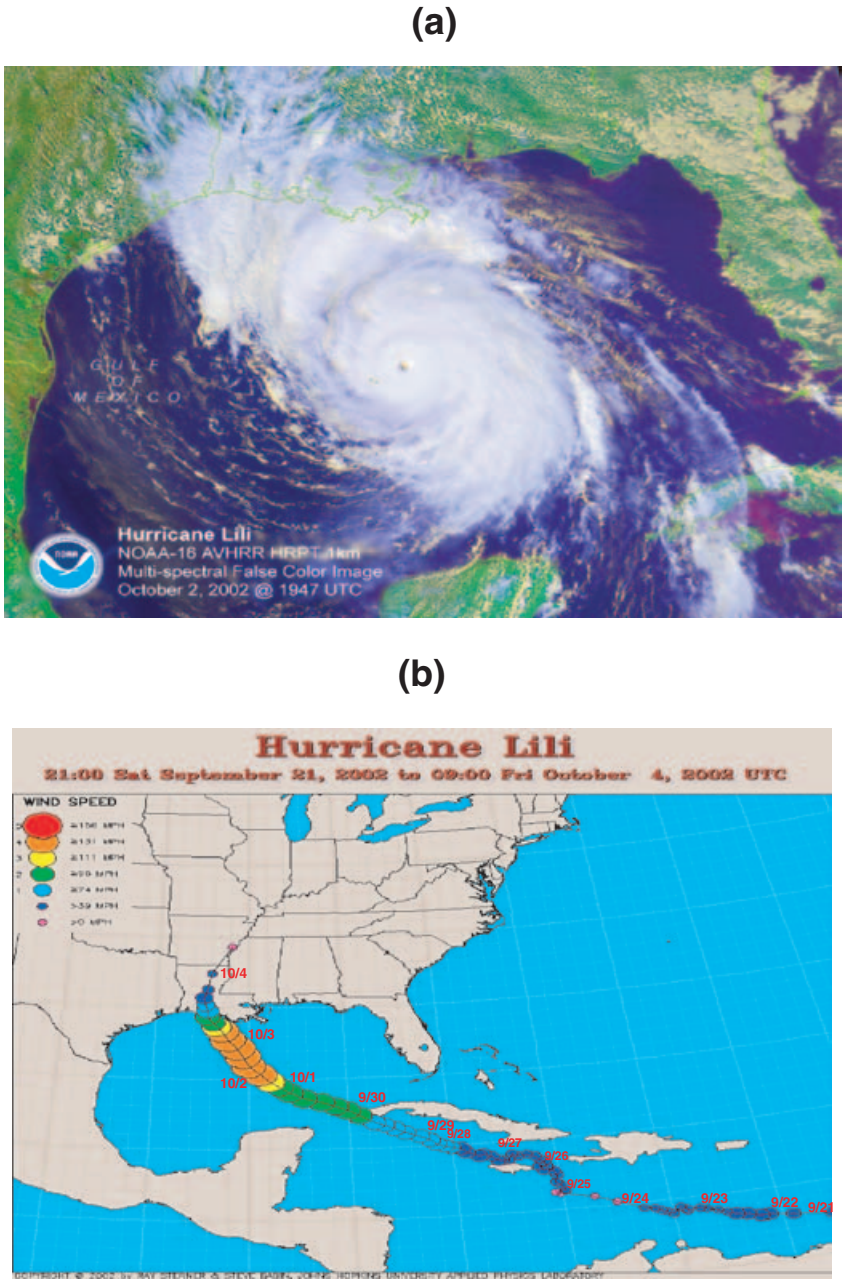

Fig 1. (a) A satellite advanced very high resolution radiometer (AVHRR) multispectral false color image of Hurricane Lili, October 2, 2002 at 1947 UTC. (b) A schematic satellite track of Hurricane Lili. (Courtesy of Ray Sterner and Steve Babin, Johns Hopkins University, Baltimore, MD.)

of the hurricane (minimum sea level pressure being the tag for storm intensity here). Our methodology is not a simple partitioning of a single equation of a model. This is based on an earlier study by Krishnamurti et al. (1996), where the partitioning of a model's history is evaluated to account for the mutual interaction among the physical and dynamical processes as the forecast proceeds in time. From very high-resolution atmospheric global spectral model forecast experiments, at the end of each time-step, the tendencies arising from each component of the model dynamics and physics are accumulated during the entire forecast period. Thus, at the end of a forecast, it is possible to assess the contributions to the total forecast tendency from the model's components of physics and dynamics. A certain feature in the model forecast (for instance, cumulus convection) is suppressed at the end of each time-step of a model forecast, for one time-step. The model is restarted at the end of each time-step with the full history of variables from a complete model run. This is done in a massively parallel computer, where one processor runs the full model and shares its history with many other processors that suppress different features of the model's physics and dynamics. The accumulated difference among such runs, with the parent model, provides the contribution of these features.

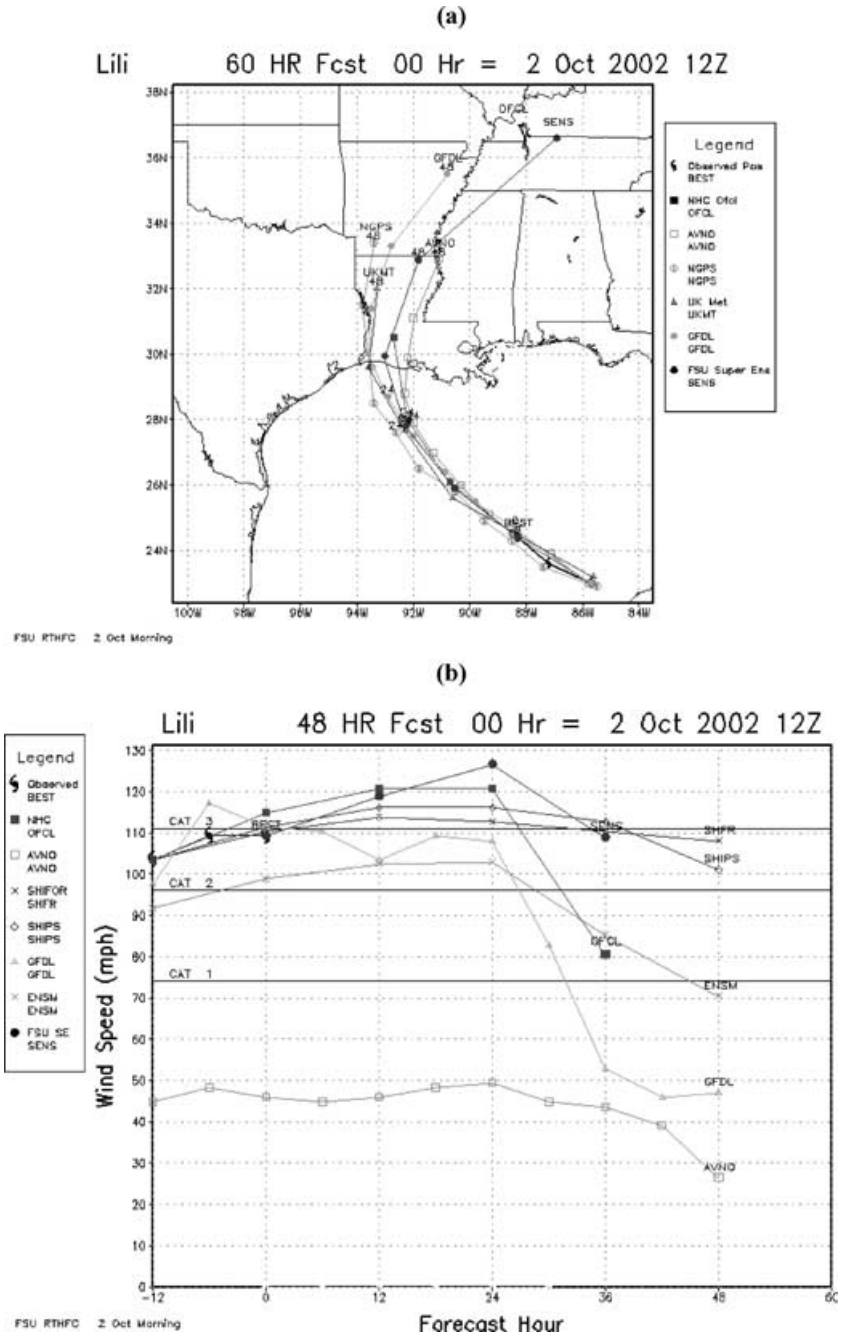

Fig 2. Multimodel and FSU superensemble based forecasts for Hurricane Lili, October 2002. (a) Track forecasts from UK Met (UK Meteorological Office), US Navy [Navy Operational Global Atmospheric Prediction System (NOGAPS)], Princeton [Geophysical Fluid Dynamics Laboratory (GFDL)], NWS [aviation run of the NCEP Medium Range Forecast (MRF) model (AVN)], National Hurricane Center Official Forecost (OFC), and the FSU superensemble (SENS). (b) Intensity forecasts (units mph) for the same models including the ensemble mean (ENSM) and the NHC in-house model Statistical Hurricane Intensity Prediction Scheme (SHIPS) and Statistical Hurricane Intensity FORecast (SHIFOR).

This is a rather straightforward procedure and is no more than a residue-free budget of a forecast. In our previous studies (Krishnamurti et al., 1996, 2004), we had labeled these as 'with and with' experiments, to contrast them from what are frequently called the 'with and without' experiments. In the latter case, one carries out experiments suppressing an area of physics entirely throughout a long-term integration. To state that 'the difference between a full experiment and an experiment where a feature is suppressed, throughout a forecast, provides information on that suppressed feature' is incorrect, because these 'with and without' experiments do not recognize that in a non-linear system all features interact, coexist and co-evolve continually. In these experiments, the differences in total tendencies from 'with and with' forecast runs provide the contribution to the tendency by one of the selected features such as advective non-linear dynamics, rest of dynamics, deep cumulus convection, large-scale condensation physics, radiative transfers and rest of physics. As an example, convection coexists continually with dynamics in a fully non-linear model and the effects of convection would be better assessed from this aforementioned tendency budget, where

the bookkeeping at the end of a time-step includes the mutual interactions among all components of the full model. Another application of the 'with and with' approach was on recurving hurricanes where questions were asked on the contributions by steering, dynamics and physics to the tropical cyclone track forecasts. Details of this work appear in O'Shay and Krishnamurti (2004). The notion of 'with and with' computations was also implicit in a recent study of Williamson (2002), where he addresses the difference between simultaneous versus sequential computations of physics and dynamics in a climate model. The first part of this paper addresses 'with and with' experiments following Krishnamurti et al. (1996). The design of these experiments is described in Section 2. The high-resolution version of the Florida State University (FSU) global spectral model and the data sets used for these studies are described in Sections 3 and 4, followed by the discussion of the results in Section 5 and conclusions in Section 6.

2. Design of experiments

To study the effect of various model components on forecasts, a number of model runs, each suppressing a specified forcing for one time-step at a time, were executed in parallel with the full model's forecast runs that carried full dynamics and physics. All model runs with partial dynamics or physics were carried out through only one time-step at a time using the parent run's (with full dynamics and physics) spectral history fields. The differences in the forecasts from the parent run and that obtained by suppressing a specified forcing were next accumulated over each 5-min interval model time-steps to provide six-hourly tendencies. These total accumulated tendencies from 'with and with' forecast runs provide the contribution to the tendency by one of the selected features such as advective non-linear dynamics, rest of dynamics, deep cumulus convection, large-scale condensation physics, radiative transfers and the rest of physics, including air–sea interaction and dry air intrusions. The selection of features could have been extended into several other categories, but were somewhat arbitrarily limited to the above and a few more.

There are three types of models that were used in the present study:

(1) a complete FSU global spectral model that includes the complete dynamics and physics (Krishnamurti et al., 1998);

(2) with and without version where a feature of the model physics or dynamics is suppressed throughout a model run;

(3) with and with version, which is identical to (2) except for the fact that at the end of each time-step the full state from the complete model, (1), is used.

The model contains a predictor corrector in its time differencing. Thus, the suppression in both (2) and (3) as well propagates the effects of a suppression of a feature to all variables. This is very robust way of addressing the contribution of a feature of a model (Krishnamurti et al., 1996). The sum of individual tendencies from each retained component does add up to the total tendency at the end of a forecast for each of the above versions of the model. Storing every time-step of information, we can carry out a precise bookkeeping of the forecast as performed by the model.

The selected features chosen for this study are grouped together in the basic prediction equations of the FSU model following Krishnamurti et al. (1998) and are shown below. The terms representing advective dynamics (AD), rest of dynamics (RD) and total physics (PH) are identified as follows: momentum equation

$$\frac{\partial V}{\partial t} = -\left[V\cdot(\nabla V)+\dot\sigma\frac{\partial V}{\partial\sigma}\right]_{\mathrm{AD}} -\left[fkV+RT'\nabla q\right]_{\mathrm{RD}}+[F]_{\mathrm{PH}}; \tag{1}$$

thermal equation

$$\frac{\partial T}{\partial t} = -\left[V\cdot(\nabla T)+\dot\sigma\frac{\partial T}{\partial\sigma}\right]_{\mathrm{AD}}+\left[\omega\frac{RT}{C_{\mathrm{p}}p}\right]_{\mathrm{RD}}+[H_T]_{\mathrm{PH}}; \tag{2}$$

moisture equation

$$\frac{\partial S}{\partial t} = -\left[V\cdot(\nabla S)+\dot\sigma\frac{\partial S}{\partial\sigma}\right]_{\mathrm{AD}} +\left[\frac{\omega}{p}\left(\frac{RT}{C_{\mathrm{p}}}-\frac{RT_{\mathrm{d}}^2}{\varepsilon L(T_{\mathrm{d}})}\right)\right]_{\mathrm{RD}}+[(H_T-H_M)]_{\mathrm{PH}}; \tag{3}$$

and surface pressure equation

$$\frac{\partial q}{\partial t} = -[V\cdot\nabla q]_{\mathrm{AD}}-\left[D+\frac{\partial\dot\sigma}{\partial\sigma}\right]_{\mathrm{AD}}. \tag{4}$$

Here, V is the horizontal wind vector; T is temperature; ω is p vertical velocity; $\dot\sigma$ is σ vertical velocity; $q=\ln p_{\mathrm{s}}$, p_{s} being the surface pressure; $S=T-T_{\mathrm{d}}$, dew point depression; F are frictional effects; H_T is the diabatic heating effect; H_M is the moisture sources and sinks effect; R is the gas constant for dry air; C_{p} is the specific heat of air at constant pressure; and $L(T_{\mathrm{d}})$ is the latent heat of water/ice at temperature T_{d}.

The forcing due to physics (PH) was further separated into forcing due to deep convection, non-convective physics, radiation, and rest of the physics, which includes shallow cumulus convection, surface fluxes (air–sea and land–sea intersection) and diffusive processes to separate the effect of various physical processes. We furthermore introduced a category 'dry air advection'. This was simply designed from the sign of moisture advection ($-V\cdot\nabla q<0$), to explore this effect.

It is of interest to note that the final partitioning information for the surface pressure tendency does not simply come from the surface pressure eq. (4) of the model alone. If that equation alone were partitioned we could only determine the contribution to surface pressure change from the advective and divergence terms of the pressure tendency equation. The partitioning, proposed in Krishnamurti et al. (1996), permits us to examine the contributions from the components of the entire system of equations of the model. Thus, we are also asking questions such as

what are the contributions to the surface pressure tendencies arising from the deep cumulus convection that appear in the thermodynamic energy eq. (2) and the moisture advection in the moisture conservation law (eq. 3). It is this type of portrayal that is presented in this paper.

3. Global spectral model

This is a comprehensive physical/dynamical model at a spectral resolution of T255 (triangular truncation at 255 waves) and 14 vertical levels. An outline of this model is presented in Appendix 1. This model has been used for numerous studies on hurricane formation and recurvature (e.g. Krishnamurti et al., 1989, 1991b, 1993, 1994) where we examined the organization of mesoscale convective precipitation within monsoon disturbances. We noted that at this resolution T255, corresponding to a transform grid separation of roughly 50 km over the tropics, the model appears to convey some useful information on the life cycle of tropical storms, hurricanes and monsoon variability. The present study is aimed at a sequence of six-hourly forecasts, where the forecast errors are expected to be quite small. The purpose of the present study is more phenomenological. Hurricane Lili underwent a major weakening with a sea level pressure rise by 23 hPa during the last 13 h prior to its landfall. The model we have put together including high-resolution physical initialization and the assimilation of a synthetic vortex provided such a pressure rise in the accumulated four six-hourly forecast segments of experiments. A detailed diagnosis of that pressure rise within the global model is the motivation of this study.

4. Data sets

Global operational analysis data sets from the National Center for Environmental Prediction (NCEP) at 1° latitude/longitude resolution and at 26 standard pressure levels are the base data sets of this study. These include the analysis of winds, temperature, humidity, mean sea level pressures, and geopotential. The sea surface temperatures (SSTs) were also extracted from the NCEP/National Weather Service (NWS) operational files. The data sets also include precipitation estimates from Tropical Rainfall Measuring Mission (TRMM) and Defense Meteorology Space Program (DMSP) satellites. The microwave instruments of these satellites provide precipitation estimates following our recent study, (Krishnamurti et al., 2001). These are six-hourly totals. This analysis also includes reconnaissance data sets from the NOAA and Air Force reserved unit aircrafts that monitored this storm over the Gulf of Mexico. These data sets were used for physical initialization of the FSU model's (Appendix 1) nowcasting of rain, following Krishnamurti et al. (1991a). This procedure assimilates the rain rates; in this process, the fields of divergence, surface pressure, heating rate and the humidity profiles undergo an initial spin-up. The correlations of the satellite-based and the model's nowcasting rain are of the order 0.9 in almost all situations (Krishnamurti et al., 2001). This provides a powerful data base for the proposed experiments. In addition to these features, we also invoke a vortex initialization following Thu and Krishnamurti (1992). Here, parameters such as storm location, size and intensity are assimilated to provide what is called a synthetic asymmetric hurricane. This feature is blended with the aforementioned large-scale analysis to ensure a smooth transition between the storm and the large-scale environment. The FSU global spectral model at a resolution of T255 was initialized by this procedure every 6 h starting from October 2, 2002 at 0000 UTC. Six such sequential analyses were prepared.

5. Discussion of forecast results

5.1. 'With and without' forecast fields

Figure 3 illustrates the results from our model when a straight 36-h forecast was carried out. The 850-hPa winds and sea level pressure, over the Gulf of Mexico region, are illustrated at intervals of every 12 h here. This forecast did show a weakening of Hurricane Lili and is, in fact, a reasonable forecast; however, the timings were somewhat incorrect. The start time of this forecast was October 2, 2002 at 1200 UTC. This forecast provided a pressure rise by 22 hPa prior to landfall between October 3 and 4 at 1200 UTC (Figs. 3b and 3d), while the actual pressure rise was 24 hPa and the landfall in fact occurred on October 3 at 1300 UTC. We found a greater improvement by conducting segments of short six-hourly forecasts. These were better suited for the type of diagnostics we present here, because they had significantly less error.

5.2. Results from 'with and with' experiments

The results from the 'with and with' partitioning for 6-h forecasts are presented here. The contribution to the surface pressure tendencies from dynamics and physics are illustrated in Fig. 4.

A pressure rise of roughly 21 hPa occurred from the total physics and dynamics over a period of 6 h. These results portray the averaged tendencies over a domain covering 26°N to 30°N latitude and 89°W to 93°W longitude.

Figure 4a indicates that the pressure rise arose largely from total dynamics (TDYN) that calls for a pressure rise by almost 36 hPa. The contributions by total physics calls for an intensification, i.e. a pressure drop by about 15 hPa. This type of information is easily extracted from the 'with and with' type of experiments used here. A simple breakdown of the dynamic contributions is shown in Fig. 4b. Here we note that the 'rest of dynamics' largely contributes a pressure rise by as much as 150 hPa over 6 h. This includes all of the dynamics excluding the advective terms. The advective non-linear dynamics calls for a drop in surface pressure by as much as 110 hPa over 6 h. Overall the total contribution by dynamics is the difference of these two large opposing contributions, calling for a pressure rise of about 36 hPa. Several of our studies (e.g. Krishnamurti et al.,

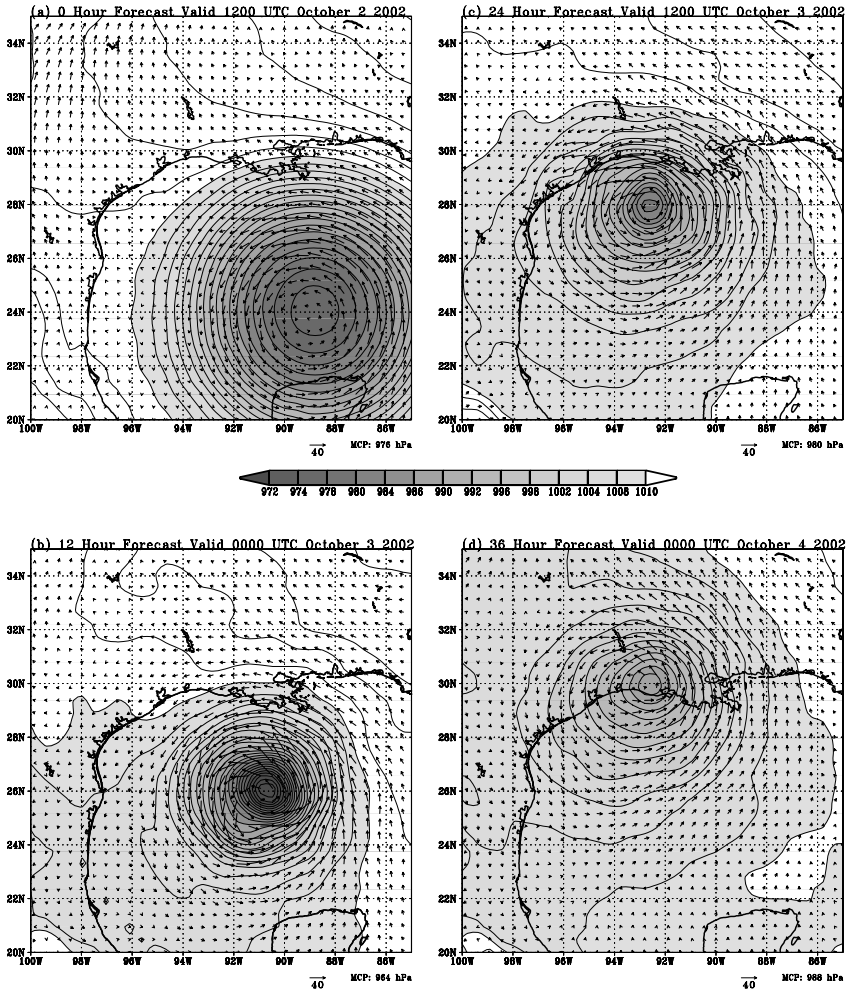

Fig 3. 12-hourly sea level pressure (hPa) and the 850-hPa wind vector (ms^{-1}) forecasts (start time, 1200 UTC, October 2, 2002). The minimum central pressure (MCP) of the forecasts is indicated at the bottom of each panel.

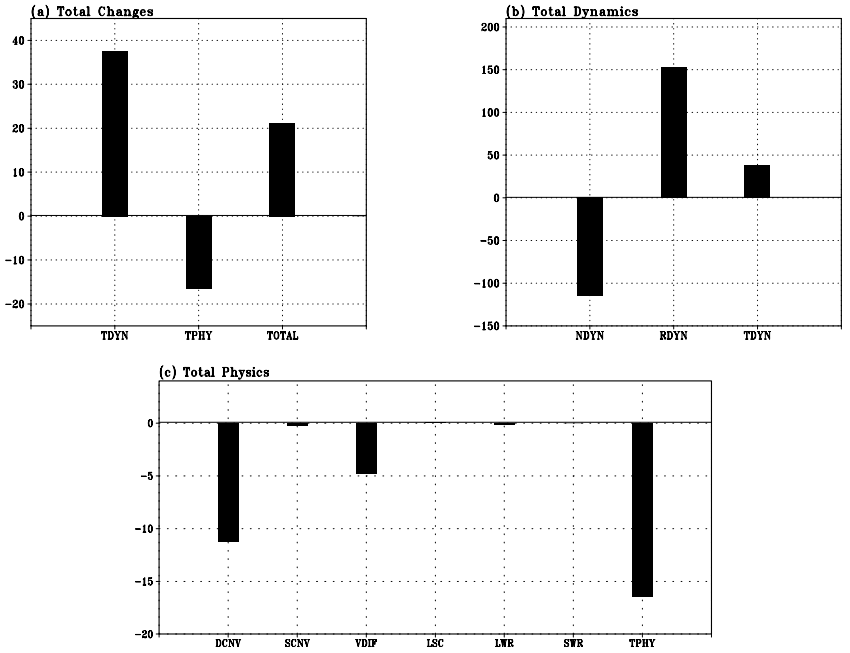

Fig 4. Contributions to the sea level pressure tendencies (hPa) over a domain enclosing 89°W to 93°W, 26°N to 30°N during a 6-h forecast period between 0600 and 1200 UTC, October 3, 2002. (a) Total dynamics (TDYN), total physics (TPHY) and the sum (TOTAL). (b) Contributions from dynamics: advective dynamics (NDYN), 'rest of dynamics' (RDYN) and the total contribution (TDYN). (c) Contributions from physics: deep convection (DCNV), shallow convection (SCNV), vertical diffusion (VDIF), non-convective rain (LSC), long-wave radiation (LWR), short-wave radiation (SWR) and the total (TPHY).

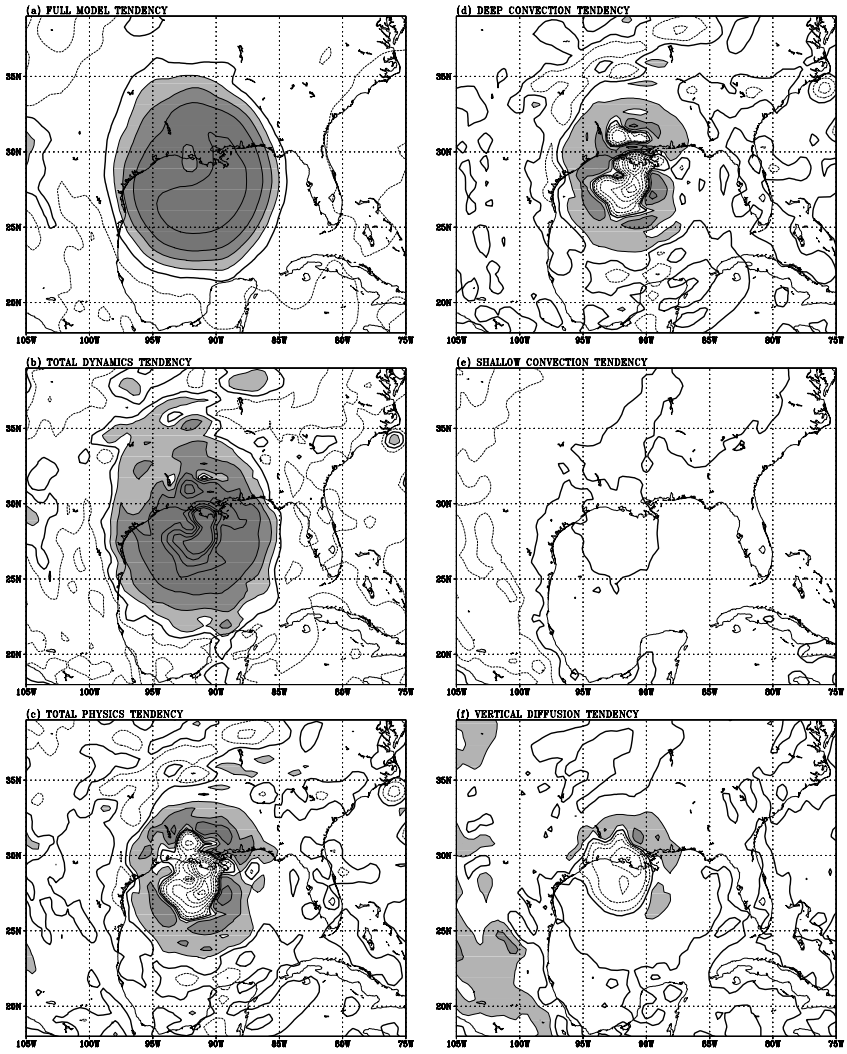

Fig 5. Contributions to the sea level pressure tendencies (hPa) during a 6-h forecast period between 0600 and 1200 UTC, October 3, 2002 from (a) full model, (b) total dynamics, (c) total physics, (d) deep convection, (e) shallow convection, and (f) vertical diffusion. The shaded area denotes positive values greater than 2 hPa (contour intervals at every two units). Negative regions are shown with dashed lines and the zero value isopleth is denoted by thick lines.

1996) on similar budget portrayals show this type of opposing contribution from the advective and non-advective dynamics.

A summary of the contributions from the physical parametrizations of the model is provided in Fig. 4c. Here we note physical processes such as deep cumulus convection and vertical eddy flux divergence of heat contribute to a deepening of the storm. These contributions to surface pressure tendencies are of the order of 12, 5, and 17 hPa for deep convection, vertical eddy flux divergence and the total physics, respectively. Results based on 6-h forecasts starting on October 3, 2002 at 0600 UTC are quite similar to those of the previous 6-h forecast (figure not shown). The essential result here is that this pressure rise is largely contributed by the 'rest of dynamics'. This rise is being neutralized somewhat by the advective dynamics and the deep cumulus convection.

Figure 5 shows the mapping of pressure tendencies arising from the full model (Fig. 5a), the total dynamics (Fig. 5b), and the total physics (Fig. 5c). These are results from the same 6-h forecasts starting on October 3, 2002 at 0600 UTC. It is clear that the full model predicted a major rise of pressure by as much as 20 hPa. This is largely contributed as a pressure rise by the total dynamics, whereas the contribution for the total physics calls for pressure fall over an inner area of the storm, roughly $r <$ 300 km, and a pressure rise in its outer peripheries ($300 < r <$ 500 km). The contribution from dynamics to this pressure rise is an interesting aspect of this partitioning.

A breakdown of the surface pressure tendencies arising from components of physical parametrizations is presented in Figs. 5d, 5e and 5f. A large proportion of the total change of surface pressure arises from deep cumulus convection, although this calls for a net deepening of the system. The contribution from shallow convection near the storm region is quite small. The divergence of vertical eddy fluxes near the storm region does contribute some deepening by about 10 hPa in 6 h. This deepening is near the storm center whereas outside a radius of roughly 300 km a pressure rise is noted in these computations. Shallow

convection seems to have a somewhat different behavior in the thermal equation. The impacts of partitioning on the thermal equation are shown in Fig. 6 for model sigma level 0.875 (roughly 875 hPa). Here, of interest are factors that contribute to the maintenance of the warm core versus those that erode it. As expected, deep convection (Fig. 6a) contributes strongly to the maintenance of the warm core; at 875 hPa, the temperature tendencies are of the order of $+2.5^{\circ}$C 6 h^{-1} in these forecasts over the region of Hurricane Lili. Shallow convection (Fig. 6b) has an overall cooling effect that is largest in the outer peripheries of the storm (-3°C 6 h^{-1}) and around -1 to -1.5°C 6 h^{-1} near the storm center. In the outer peripheries of this storm, shallow convection contributes to a net sea level pressure rise and to an overall cooling.

Large-scale condensation is invoked under conditions of ascent of absolutely stable air under saturated conditions. Figure 6c shows a net strong cooling at the 875-hPa level to the northern and eastern peripheries of the storm. This cooling is as large as -3°C 6 h^{-1}. This result is not surprising because those were the regions of the largest non-convective rain where the moist adiabatic lapse rate was noted to be steeper than the model's prevailing lapse rate.

The results of the thermal equation's budget are presented in Fig. 7. The total temperature tendency (Fig. 7a) shows a cooling tendency (-12°C 6 h^{-1}) for total dynamics and a warming ($+10.5^{\circ}$C 6 h^{-1}) by the total physics. The net result is a slight overall cooling of temperature at the 875-hPa level by about 1.5°C 6 h^{-1}. This overall budget also confirms the role of the total dynamics playing a key role in the weakening of Hurricane Lili. The net dynamical contribution was an overall cooling by about -10°C 6 h^{-1} (Fig. 7b). This is believed to be largely a consequence of wind pressure adjustment that is discussed in Section 5.5. The partitioning of the physics is illustrated in Fig. 7c. Here the net effect is a warming by about $+10.5^{\circ}$C 6 h^{-1}. This is largely from the effects of deep cumulus convection, which contributes a warming by about $+12^{\circ}$C 6 h^{-1} and is slightly counteracted by shallow convection, -1.5°C 6 h^{-1}, and by large-scale condensation, -0.2°C 6 h^{-1}. Most of these cooling effects by shallow convection and large-scale condensation arise from just outside the hurricane core ($r > 300$ km) whereas the effects of deep convection are centered over the storm at roughly $r < 500$ km.

5.3. *Role of dry air advection from the north*

Satellite imagery provided some indication that dry air was being advected southwards towards Hurricane Lili during the time of its weakening and landfall. Figure 8 illustrates a water vapor image obtained from GOES 8. In this instance, a time-lapse movie of images from the water vapor channel around this time showed that the dry air was in fact well separated for Hurricane Lili during its weakening. Seeing a dry air swath on a satellite photograph does not necessarily imply that it was supporting

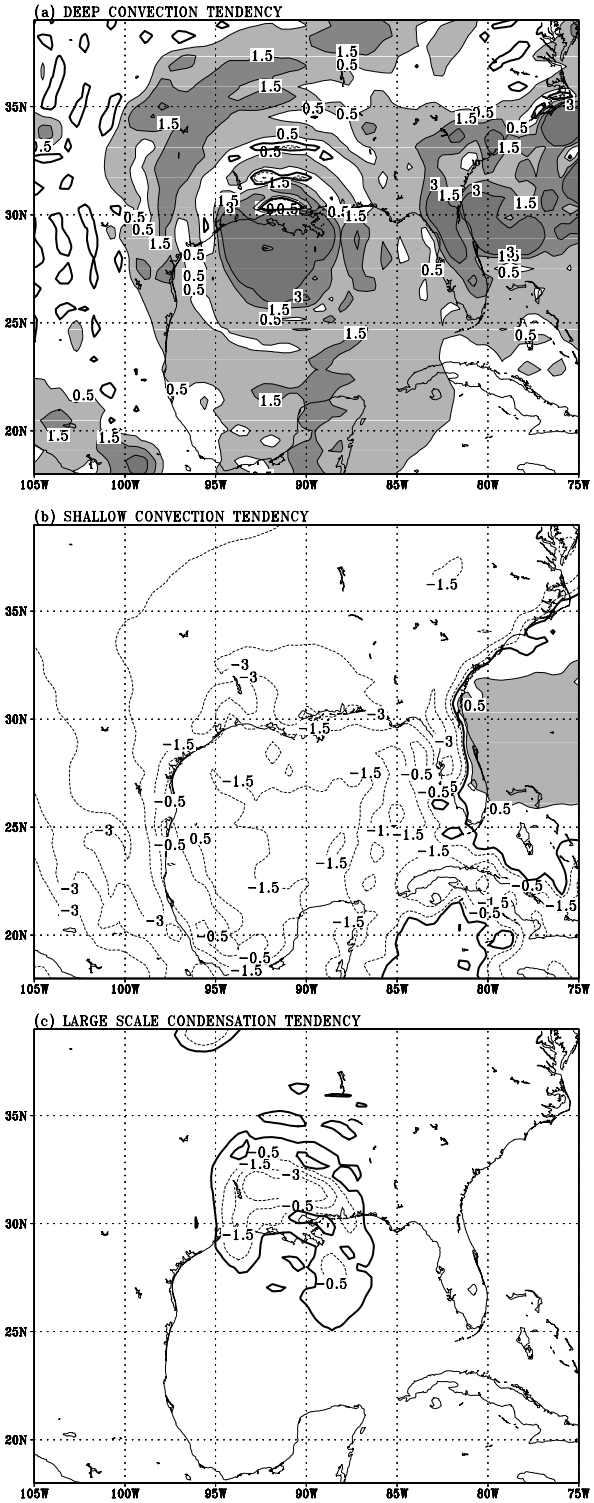

Fig 6. Contributions to the temperature tendencies (K) at $\sigma = 0.875$ level during a 6-h forecast period between 0600 and 1200 UTC, October 3, 2002 from (a) deep convection, (b) shallow convection, and (c) large-scale condensation. The shaded area denotes positive values greater than 0.5 K. Negative regions are shown with dashed lines and the zero value isopleth is denoted by thick lines.

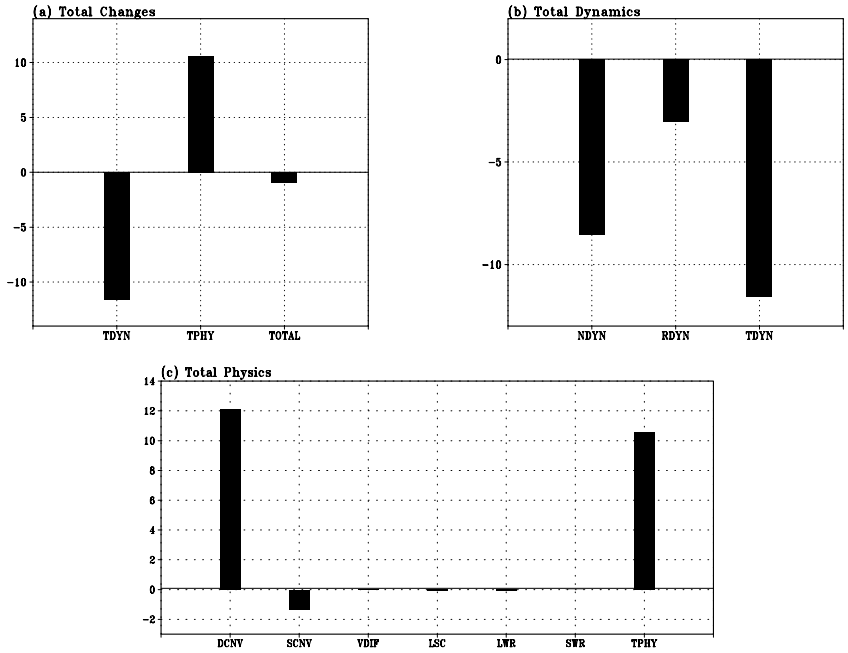

Fig 7. Same as Fig. 4 except for contributions to the temperature tendencies (K) at $\sigma = 0.875$.

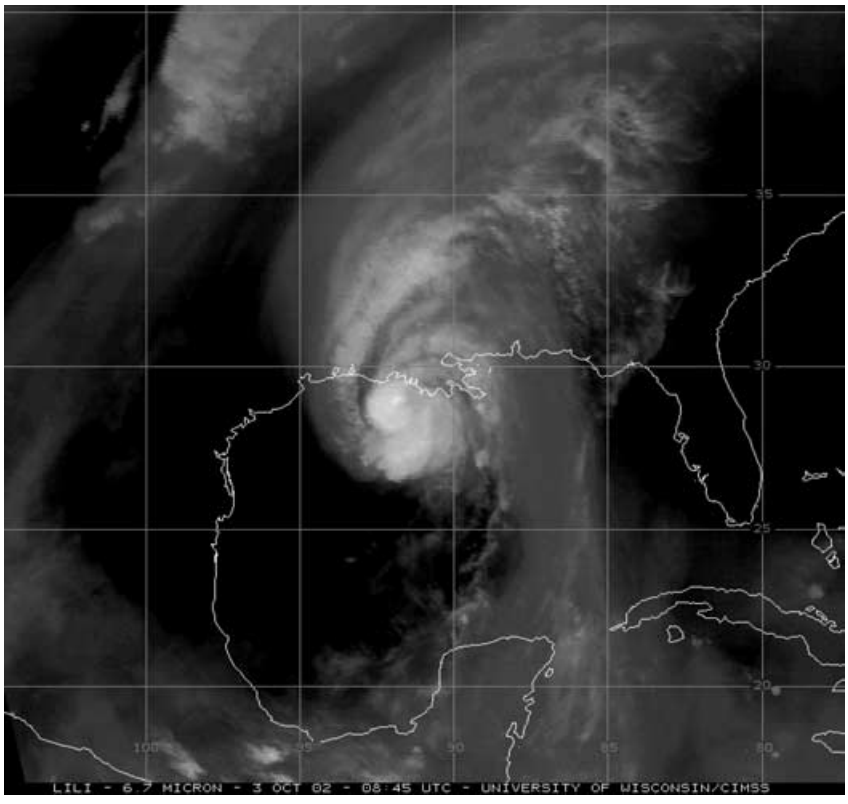

Fig 8. Water vapor imagery from GOES 8 for October 3, 2002 at 0845 UTC.

the mechanism for the weakening of the storm. This issue was also addressed by the proposed 'with and with' approach. In order to address this, we suppressed values of $-V \cdot \nabla_q$ less than zero in the one time-step of partitioned forecasts using our proposed method. This was specifically designed to set to zero the value of $-V \cdot \nabla_q$ within a 500-km radius of this storm. Figures 9 and 10 illustrate a sequence of 12-hourly forecast fields of specific humidity changes and the sea level pressure tendency arising from the contributions of dry air advection alone. These computations were carried out within the inset rectangle where

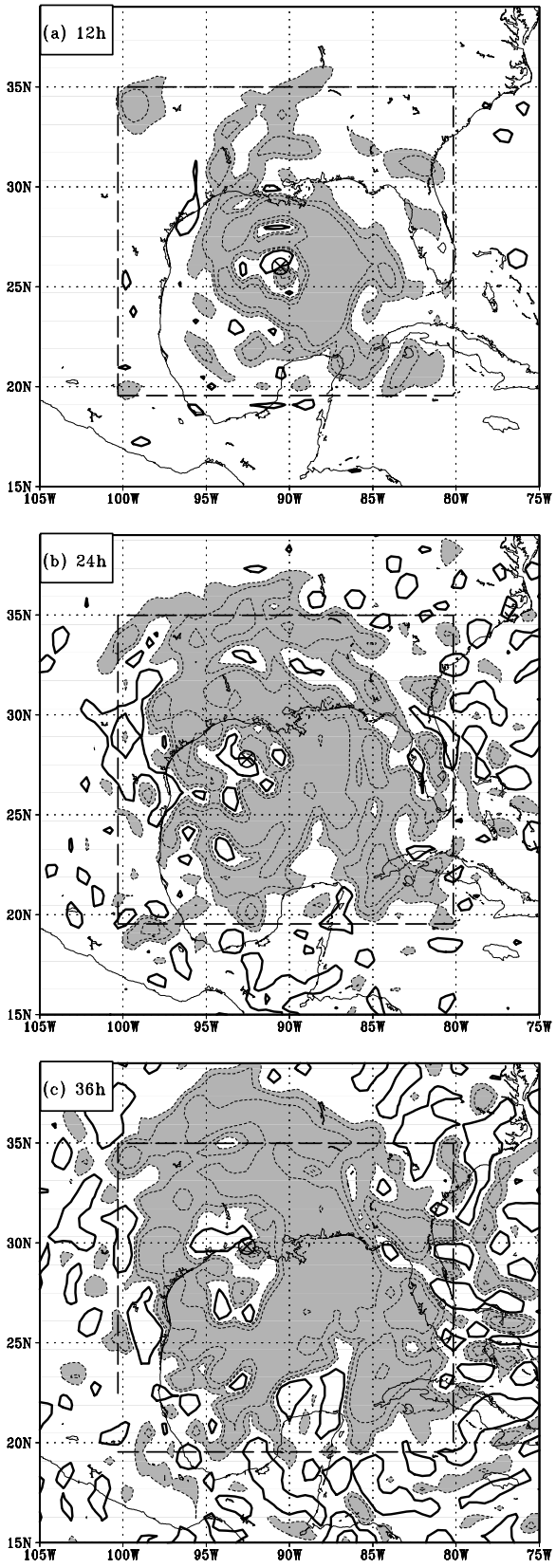

this partitioning was executed. This was done for all vertical levels of the model. Here we show the contribution to the sea level pressure tendencies from the term, i.e.

$$\left.\frac{\partial p}{\partial t}\right)_{\text{dryairadvection}} = \left.\frac{\partial p}{\partial t}\right)_{\text{total}} - \left.\frac{\partial p}{\partial t}\right)_{\text{excludingdryairadvection}}. \qquad (5)$$

Overall we do see a drying by roughly 2 to 3 g kg^{-1} of moisture by hour 36 and a pressure rise of roughly 2 hPa from the dry air advection into the storm. This suggests that the effect of dry air advection into the inner storm area was not a critical factor in the observed pressure rise by almost 22 hPa. This conclusion can be questioned on the merits of the resolution of the model near 30°N. The spectral transform resolution of the T255 model was close to 50 km and may not have been sufficient to capture incursion of a very narrow swath of dry air wrapping into the storm. This resolution issue could, of course, be true for many of the terms examined in this paper. Satellite water vapor imagery (Fig. 8) supports our contention that the dry air was in fact well separated from the storm, and the computations confirmed the passive role of dry air advection in the weakening of Hurricane Lili.

The results of one 6-h segment are illustrated here to discuss the impacts of dry air advection. This was done in both the 'with and without' and the 'with and with' strategies. Figure 11a shows a more robust response from the 'with and without' approach where the six-hourly impact on sea level pressure tendency was only around 1 hPa. The same experiment repeated in the 'with and with' approach (Fig. 11b) showed only a trivial local response. Our conclusions are that the dry air advection was not an important contributor to the observed pressure rise of Lili.

5.4. *Role of air–sea interaction, surface moisture fluxes and the SST fields*

About a week before Lili, Tropical Storm Isidore also affected the northern Gulf of Mexico coast, and also made landfall in Louisiana. Isidore caused a cooling of the waters of the northern and central Gulf of Mexico. These cooler SSTs were still present when Lili traversed the area. In our model integrations we used the SST fields for October 2 and 3, 2002. These daily fields, shown in Figs. 12a and 12b, were obtained from the NOAA data archives. Between October 2 and 3, where the storm was

Fig 9. Differences in specific humidity (gm kg^{-1}) at the 850-hPa level from control (CTL) experiment and another experiment that excludes dry air advection (CTL-QHADV). This difference is the contribution by dry air advection. Panels show 12-hourly forecasts (start time, 1200 UTC, October 2, 2002). Negative regions are shaded and shown with dashed lines (contour intervals at every one unit) and the zero value isopleth is denoted by thick lines.

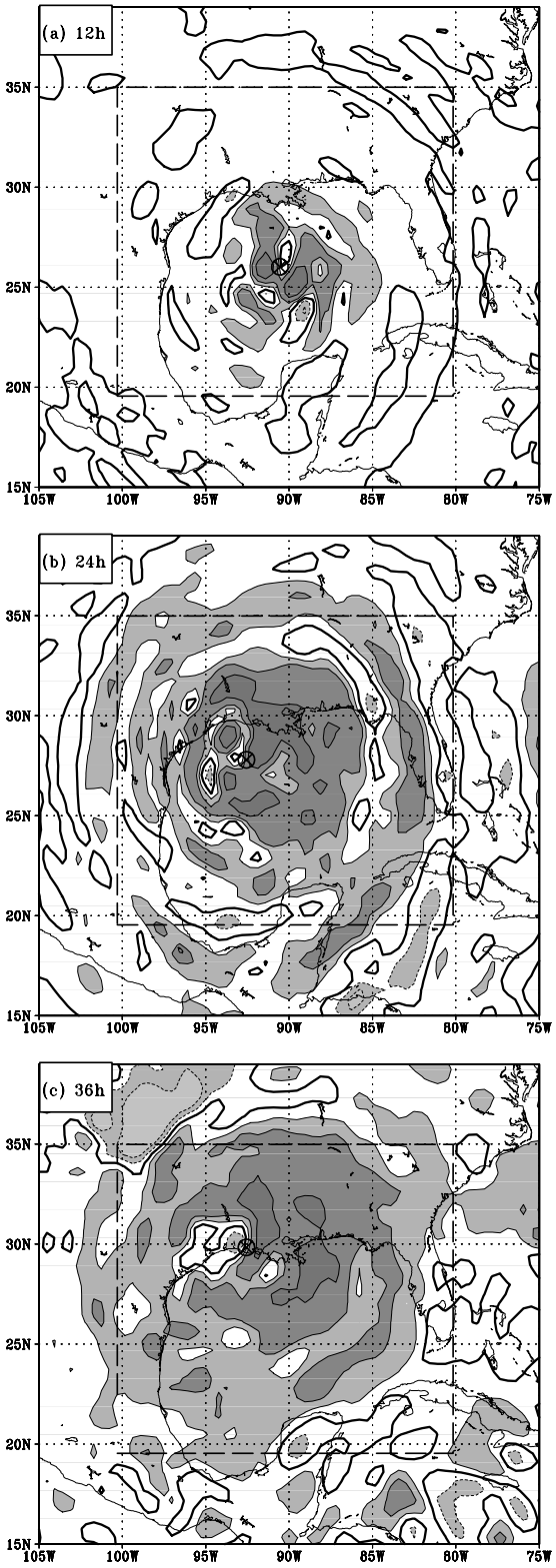

Fig 10. Same as Fig. 9 except for differences in sea level pressure (hPa). Shaded regions correspond to magnitudes greater than 0.5 hPa, negative regions are shown with dashed lines and the zero value isopleth is denoted by thick lines.

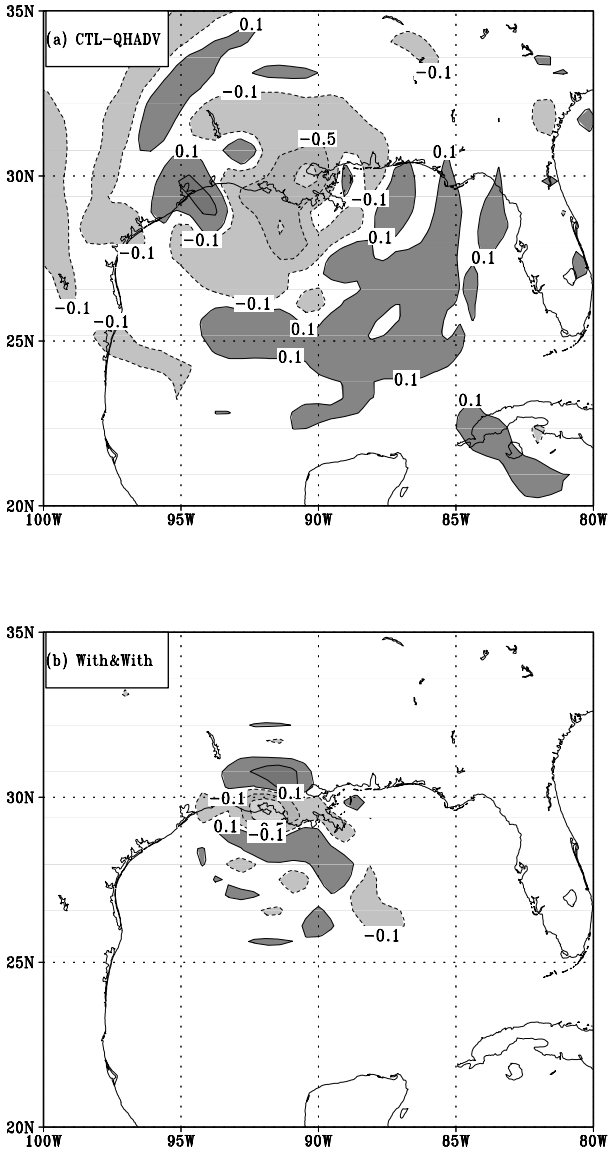

Fig 11. A comparison of sea level pressure impacts (hPa 6 h^{-1}) from the exclusion of dry air advection for (a) 'with and without' versus (b) 'with and with' experiments. Shaded regions correspond to magnitudes greater than 0.1 hPa, negative regions are shown with dashed lines and the zero value isopleth is denoted by thick lines.

exhibiting a major weakening from a category 4 storm to a category 1 storm (as landfall occurred), the SSTs did exhibit cooling (Fig. 12c). However, these SSTs show only a very slight cold feature in most of the storm track from its most intense phase to its weakest phase over the ocean. The cooling shown in Fig. 12c is at most of the order of 0.6°C. Another SST data set, not used in the present study, was highlighted by Shay et al. (2003), where they suggested that these cold SSTs might be a possible contributor to the weakening of Hurricane Lili. This field is shown in Fig. 12d. The fields we used and those of Shay et al. (2003)

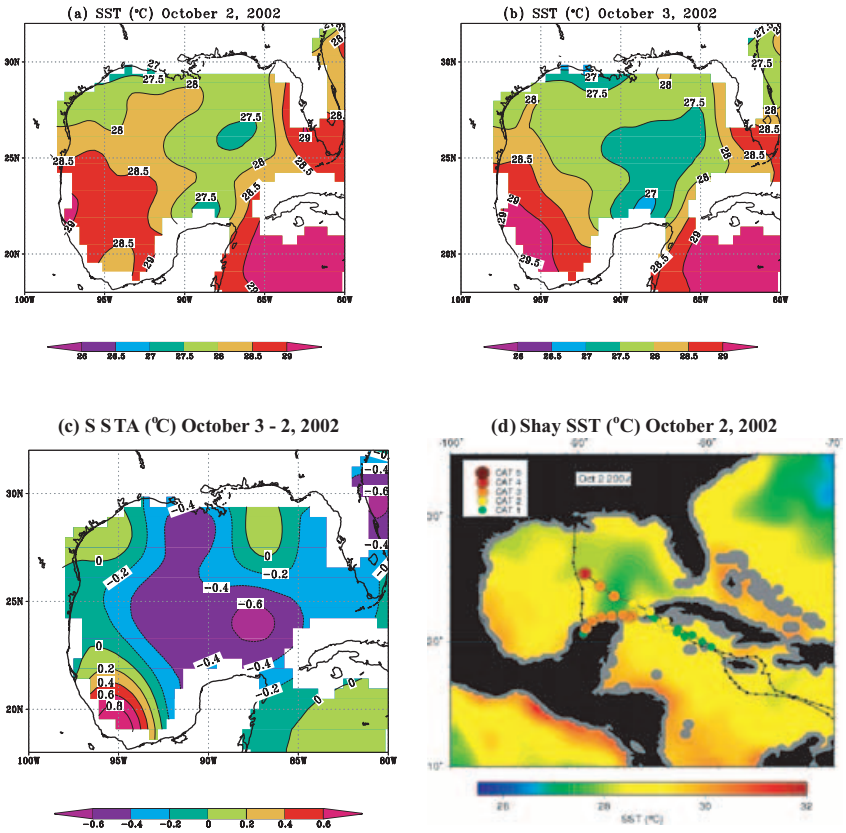

Fig 12. SST used in the experiments: (a) October 2, 2002; (b) October 3, 2002; (c) differences in SST between October 3 minus October 2, 2002; (d) the SST field for October 2, 2002 based on Shay et al. (2003). All units are in °C.

look quite comparable. Thus, we feel that the sensitivity studies portrayed here have used reasonable fields of SST.

We then carried out a 'with and without' experiment where the effects of moisture flux from the ocean were suppressed for an entire 36 h of long integration. This 'with and without' approach entailed the following two experiments: (1) a full model run; (2) a model run that suppresses the surface moisture flux. The difference of results from (2) minus (1) denotes the effects of surface humidity flux on the surface pressure tendencies in this context. This was also repeated using the more correct 'with and with' strategy as well. Figure 13 illustrates the results from a continuous integration through 36 h of forecast. Here, 12-hourly forecast panels are illustrated. In this straight run, we noted a pressure rise by almost 20 hPa in 36 h. This appears quite promising as an explanation for the observed pressure rise, but this experiment did not allow the coexistence of physics and dynamics and required a re-examination of the same within the 'with and with' context.

Three series of experiments were conducted to explore the effect of oceanic moisture fluxes on the surface pressure tendencies. In these, we varied the 'with and with' stream of computations after one, two and four time-steps successively. In all of these experiments we noted a very small effect on the sea level pressure tendency. Figures 14a and 14b show the results from a segment of 6-h forecasts from the 'with and without' and the 'with and with' strategies. The field of impact is larger on the 'with and without' experiment (Fig. 14a), roughly 7 hPa 6 h^{-1} compared to the 'with and with' impact shown in Fig. 14b, which had an impact of roughly 1 hPa 6 h^{-1}. However, for reasons stated above we discounted the impacts of the 'with and without' experiments. Overall we note that the effects of suppression of the surface humidity fluxes, where the model variables and the imposed SSTs were used to compute these contributions of surface humidity flux, did not contribute to a substantial rise of surface pressure. The full non-linear dynamics of the model, where the surface fluxes are allowed to interact with the rest of the model, shows a pressure rise by only a few hPa in 36-h integrations (carried out in these sequential six six-hourly forecast experiments).

5.5. *Role of the 'rest of dynamics'*

'Rest of dynamics' is all other dynamics in the model that do not invoke the advective non-linearities. Largely this includes the divergence term of the vorticity equation. The average vertical motion in an inner domain of 1000 km^2 around the storm exhibited increased downward motion during the weakening phase of Lili. In Fig. 15a we illustrate the model's predicted 'storm-relative' flow field at the 850-hPa level along with the vertically integrated vertical velocity $\hat{\sigma}$ (18-h forecasts from October 2,

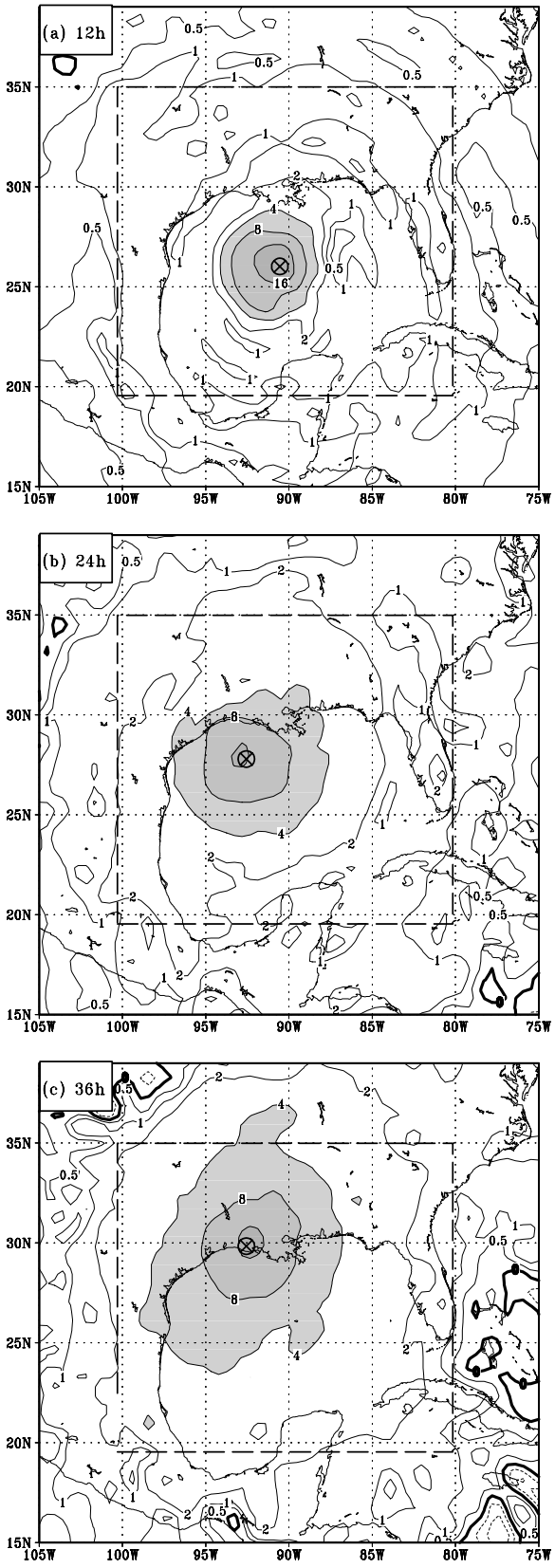

Fig 13. Impact of surface humidity flux on sea level pressure (units hPa) at intervals of 12 h in 'with and without' type forecast experiments (start time, 1200 UTC, October 2, 2002). Shaded regions correspond to values greater than 4 hPa, negative regions are shown with dashed lines and the zero value isopleth is denoted by thick lines.

2002 at 1200 UTC). The coloring illustrates regions of rising and sinking motions. Yellow and red coloring show rising areas and white to blue are regions of descent. A major inflow channel extends north between 85° and 90°W longitudes. This channel

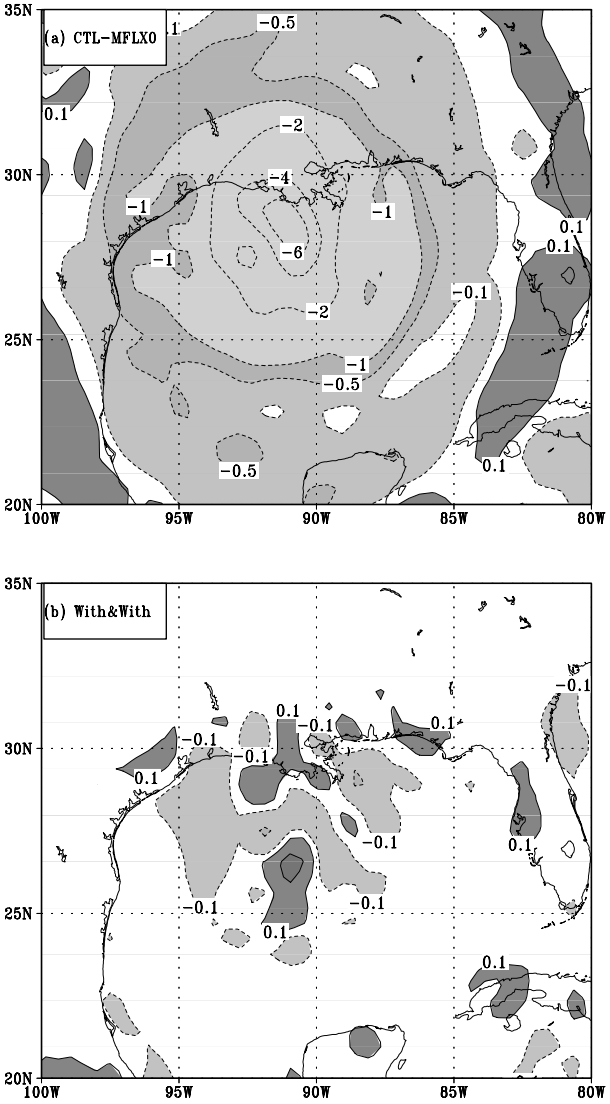

Fig 14. A comparison of sea level pressure impacts (hPa/6 hr) from the exclusion of surface humidity fluxes for (a) 'with and without' versus (b) 'with and with' experiments. Shaded regions correspond to magnitudes greater than 0.1 hPa, negative regions are shown with dashed lines and the zero value isopleth is denoted by thick line.

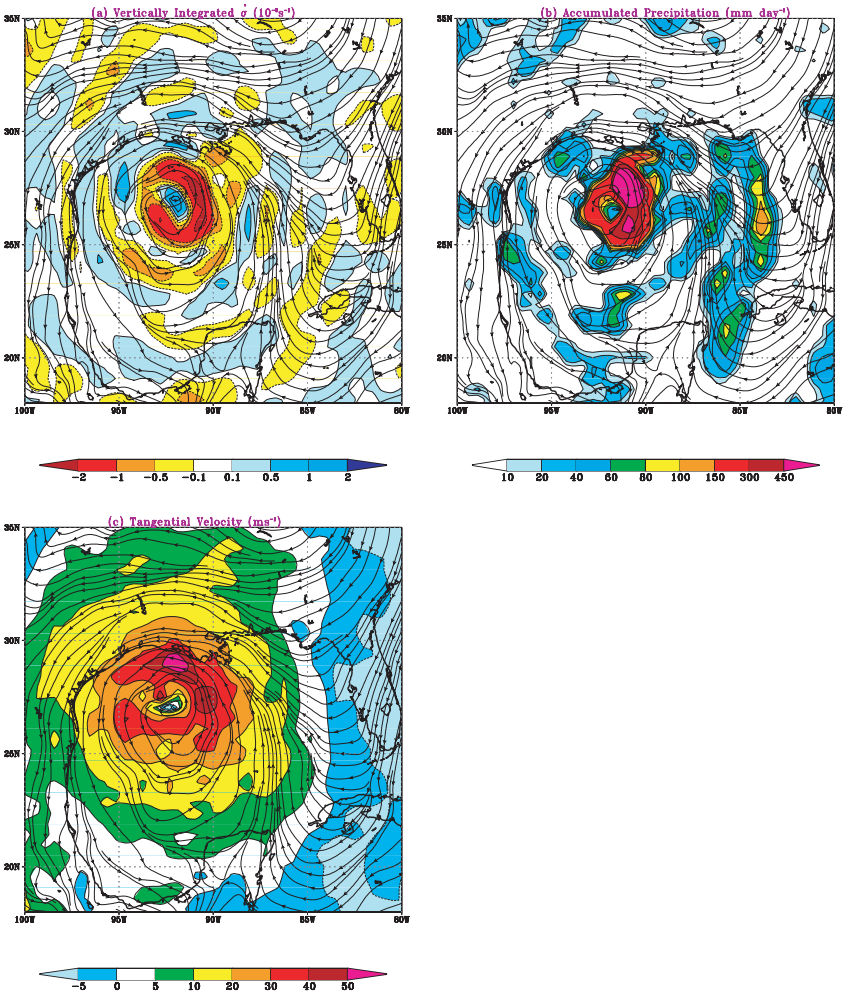

Fig 15. Hour 18 forecast fields (start time, October 2, 2002 at 1200 UTC) from the full model (resolution T255) of (a) vertically integrated vertical velocity $\dot{\hat{\sigma}}$ (units 10^{-5} s^{-1}), (b) 1-h accumulated precipitation between hours 18 and 19 of forecasts (units mm d^{-1}), and (c) tangential velocity (units m s^{-1}) at 850-hPa level. Superimposed on each panel are the storm-relative streamlines at the 850-hPa level. All fields are in storm-relative coordinates.

contains moderate rising motions as this air enters the storm inner core circulation. This entire channel is covered with several pockets of heavy rain and clouds in the model's forecasts. This field of instantaneous 1-h precipitation (Fig. 15b), from the full model output, between 0600 and 0700 UTC (hour 18 to hour 19 of the forecast) shows totals in units of mm d^{-1}. The largest rainfall amounts are in the eye wall region, around 450 mm d^{-1}. The south-eastern rain band along the inflow channel contains precipitation amounts in excess of 40 mm d^{-1} over most of this region. Overall, this model depiction of rain carries many of the features seen in the satellite imagery. Figure 15c illustrates the 850-hPa level relative streamlines and the tangential velocity, predicted by the model at the same hour 18 of forecast. The highest wind speed is around 50 ms^{-1}, which is 6 h after the initiation of the weakening phase of Hurricane Lili in the model simulation. Most of the strong winds lie between 30 and 50 ms^{-1} in the eastern and northern sector of the storm.

We next ask the question what is this 'rest of dynamics' that can affect the weakening of a storm? To pursue this question we have examined a number of areas of model output histories.

The 'rest of dynamics' in the momentum equation is $fk \times \backslash V + RT^* \nabla q$, where $\backslash \mathbf{V}$ is the vector horizontal wind on a model sigma surface, T^* is a global area averaged temperature at a sigma level and q is the log of the surface pressure. Between these two terms $RT^* \nabla q$ is smaller in magnitude. This translates in the vorticity equation, for the $x - y - \sigma$ frame of reference, to $-\nabla \cdot \mathbf{fV} - \mathbf{k} \cdot \nabla \times \mathbf{RT}\nabla\mathbf{q}$. Furthermore an approximate relation

$$\zeta_{\mathbf{a}} = \frac{\mathbf{1}}{\mathbf{r}} \frac{\partial \mathbf{M}}{\partial \mathbf{r}},$$

where

$$\zeta_{\mathbf{a}} = \frac{\partial \mathbf{V}_\theta}{\partial \mathbf{r}} + \frac{\mathbf{V}_\theta}{\mathbf{r}} + \mathbf{f}$$

and $\mathbf{M} = \mathbf{V}_\theta \mathbf{r} + \mathbf{fr}^2/2$, enables us to see the rest of dynamics in light of angular momentum gradients. If we take $\mathbf{k} \cdot \nabla \times$ of the equation of motion, we obtain the vorticity equation; if we multiply the equation of motion by a radial distance $\mathbf{r}$ from the storm center, we obtain the angular momentum equation. The two similar terms categorized as 'rest of dynamics' are $-\nabla \cdot \mathbf{fV}$ in the vorticity equation and $-\mathbf{V} \cdot \nabla(\mathbf{fr}^2/2)$ in the angular momentum

equation. These terms were the larger contributors to the surface pressure changes in Lili than all other terms in the 'rest of dynamics'. This separation of the Coriolis force term in the momentum equation from the non-linear advection term is passed on to the corresponding angular momentum equation where $-\mathbf{V} \cdot \nabla(\mathbf{V}_\theta \mathbf{r})$ translates to advective dynamics, and $-\mathbf{V} \cdot \nabla(\mathbf{fr}^2/\mathbf{2})$ translates to the 'rest of dynamics'. The pressure torques of the angular momentum equation also belong in the 'rest of dynamics' category; these were very small because of the essential azimuthal symmetry of the pressure field around the storm center for $\mathbf{r} <$ 500 km. Here $\mathbf{V}_\theta$ is this tangential velocity and $\mathbf{r}$ is the radial distance from the storm center. All of these were calculated in storm-relative coordinates. It should be noted that $(fr^2)/2$ does not vary with height. However, $V_\theta r$ does vary slightly over the lower troposphere with the largest values of the angular momentum coinciding with the largest values of the tangential velocity V_θ. This occurs roughly 1 km above the ocean or near 900 hPa.

The inflow channel was already present when Hurricane Lili attained category 3 winds on October 2, 2002 at 1200 UTC. If no pressure torques or frictional torques were present, then the parcels moving along this inflow channel would have resulted in infinite winds near $\mathbf{r} = 0$. To have attained only category 3 winds on October 2, 2002 at 1200 UTC, this storm had already faced some strong frictional torques. Frictional torques in the model are provided by surface friction and by the cloud turbulence (vertical diffusion) in the cloudy environment along these inflow channels. In the model we have subgrid-scale vertical diffusion and the same parametrized for the representation of shallow convection. On October 2, 2002 at 1200 UTC, these processes were holding the storm in an equilibrium stage with respect to category 4 winds. Although very large values of total angular momentum were brought into the inner radii of the inflow channels (in storm-relative coordinates), a loss of this angular momentum from vertical transports to higher vertical levels continually occurs. The relative angular momentum in fact increases as we proceed inward; to a first order, this increase is attributed to the losses encountered by the Earth's angular momentum of inward moving parcels. The manner in which the inward moving Earth's angular momentum is lost (by exchange to relative angular momentum, by surface friction, by cloud friction, by pressure torques, and by larger-scale vertical transports) eventually determines the strength of any hurricane.

Large outer angular momentum air enters the storm inner circulation via these channels. This momentum is carried up by vertical advection and vertical diffusion. The horizontal advection of relative angular momentum generally cancels the vertical advection of relative angular momentum. The extensive spread of downward motions in the storm environment suppresses deep convection while the shallow convection increases gradually. Our thermodynamic budgets show that one contributor to the erosion of the warm core of Lili was from shallow convection. A preponderance of shallow convection in the storm's outer area (outside the inner heavy rain area) was noted in the model. In our model formulation, we do not include the effects of vertical eddy flux of momentum (or angular momentum) by shallow clouds. The only visible effects are the transports by larger-scale vertical motions and by vertical diffusion.

In Fig. 16 we show six panels illustrating the fields, for Hurricane Lili, of total angular momentum (Fig. 16a), relative angular momentum (Fig. 16b), Earth angular momentum (Fig. 16c), advection of the total angular momentum (Fig. 16d), advection of relative angular momentum (Fig. 16e), and advection of Earth angular momentum (Fig. 16f). These are all shown in storm-relative coordinates at the 850-hPa level. The 850-hPa streamline of the flows in storm-relative coordinates are also displayed in each of these panels. These are model-based fields at hour 18 of forecast when Lili had started to weaken on October 3, 2002 at 0600 UTC. Our interest here is to show a major component of the 'rest of dynamics' that contributed significantly to the decay of intensity of Lili.

Figure 16a shows the field of total angular momentum $\mathbf{M}$ at the 850-hPa level for October 3, 2002 at 0600 UTC. At first sight, this appears as a non-descriptive field with $\mathbf{M}$ increasing outward (towards increasing radius $\mathbf{r}$), but a closer inspection of the relative streamline at 850 hPa and the isopleths of $\mathbf{M}$ shows some very interesting features. The flow field systematically intersects the line of total angular momentum, thus contributing to regions of positive and negative angular momentum advection into and out of the storm. There appears to be one prominent channel of strong inflow from south to north towards the storm center in these relative streamlines. Along this channel, high values of outer total angular momentum are transported.

Figure 16b shows the field of the relative angular momentum, $\mathbf{rV}_\theta$ (in $\mathrm{m}^2\ \mathrm{s}^{-1}$), near the region of strongest winds (yellow coloring). Relative angular momentum decreases at increasing radii from the storm center; over regions of anticyclonic flows (with respect to the storm center) to the east (blue coloring) the relative angular momentum is negative. For advection of the relative angular momentum by these storm-relative winds, the crossing of the streamline across lines of constant relative angular momentum is relevant. The largest values of $\mathbf{rV}_\theta$ are noted close to the mid-maximum of the tangential velocity. The Earth's angular momentum, $\mathbf{fr}^2/2$, shown in Fig. 16c, shows increasing values away from the storm center as $\mathbf{r}^2$ increases. Here again, of interest is the manner of crossing of the streamlines in storm-relative coordinates with respect to the isopleths of the Earth's angular momentum. This crossing can be viewed by the advection of total, relative, and Earth angular momentum, shown in Figs. 16d, 16e, and 16f, respectively. The patterns of advection of total angular momentum and of the Earth's angular momentum largely show negative values for advection west of the storm's central longitude and positive values to the east. The largest negative values of advection reside to the north-west of the storm center. Thus, the large negative value of advection in Lili is of major interest here because the incursion of negative Earth angular momentum from the north-west enters the storm center. We expect

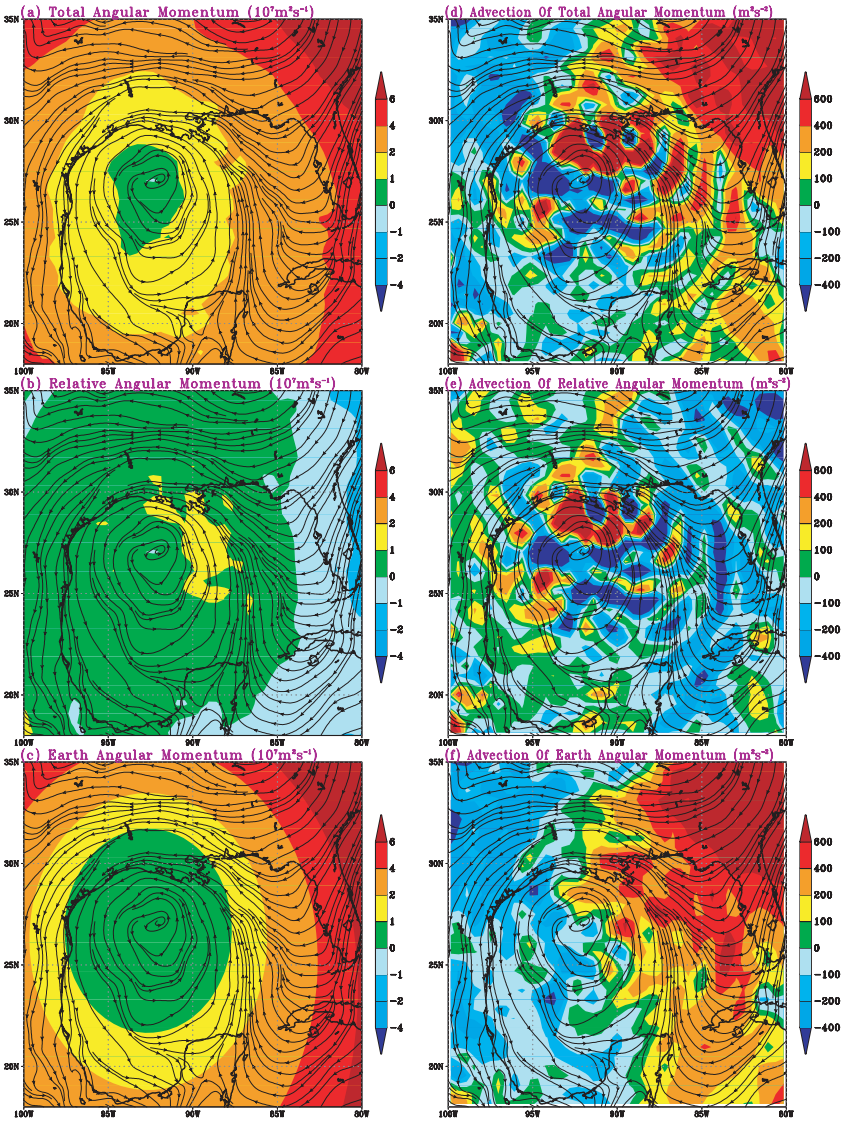

Fig 16. Hour 18 forecast fields (start time, October 2, 2002 at 1200 UTC) from the full model (resolution T255), at the 850-hPa level: (a) total angular momentum (units 10^7 m^2 s^{-1}); (b) relative angular momentum (units 10^7 m^2 s^{-1}); (c) Earth angular momentum (units 10^7 m^2 s^{-1}); (d) advection of the total angular momentum (units m^2 s^{-2}); (e) advection of relative angular momentum (units m^2 s^{-2}); (f) advection Earth angular momentum (units m^2 s^{-2}). All panels include storm-relative streamlines at the 850-hPa level. All fields use storm-relative winds.

these features to last for several hours since this picture is in storm-relative coordinates. This feature of the low angular momentum air entering the storm center from the north-west is quite similar to the incursion of a dry air plume into the storm from the north-west, which was depicted in the water vapor imagery shown earlier (Fig. 8). The advection of Earth's relative angular momentum falls within our 'rest of dynamics' category, whereas the incursion of dry air is part of our thermodynamic partitioning of model contributions to the surface pressure tendencies. Also shown in Fig. 16e is the field of advection of relative angular momentum. This field has multiple coloring to the north and west of the storm. This term is derived from the advective dynamics that contributed to a net pressure drop when Lili was weakening. Several positive and negative pockets of relative angular momentum advection are found around the storm. These pockets are largely counteracted by the vertical advection of relative angular momentum (not shown here), thus this term did not contribute to the demise of Lili.

It is of some interest to compare the fields of angular momentum advection of Lili with other hurricanes. A vast data set was recently assimilated by our group for Hurricanes Erin, Gabrielle, and Humberto of the 2001 season (Kamineni et al., 2003). This includes the dropwindsonde from as many as six research aircraft. These three storms were at different stages of their life cycles (Pasch et al., 2004). These three storms were showing hurricane force winds during the 24 h after the initial analysis time portrayed here.

Using the analyses for Hurricanes Erin, Gabrielle, and Humberto we prepared the fields of advection of total angular momentum (left panels of Fig. 17) and of the Earth's angular

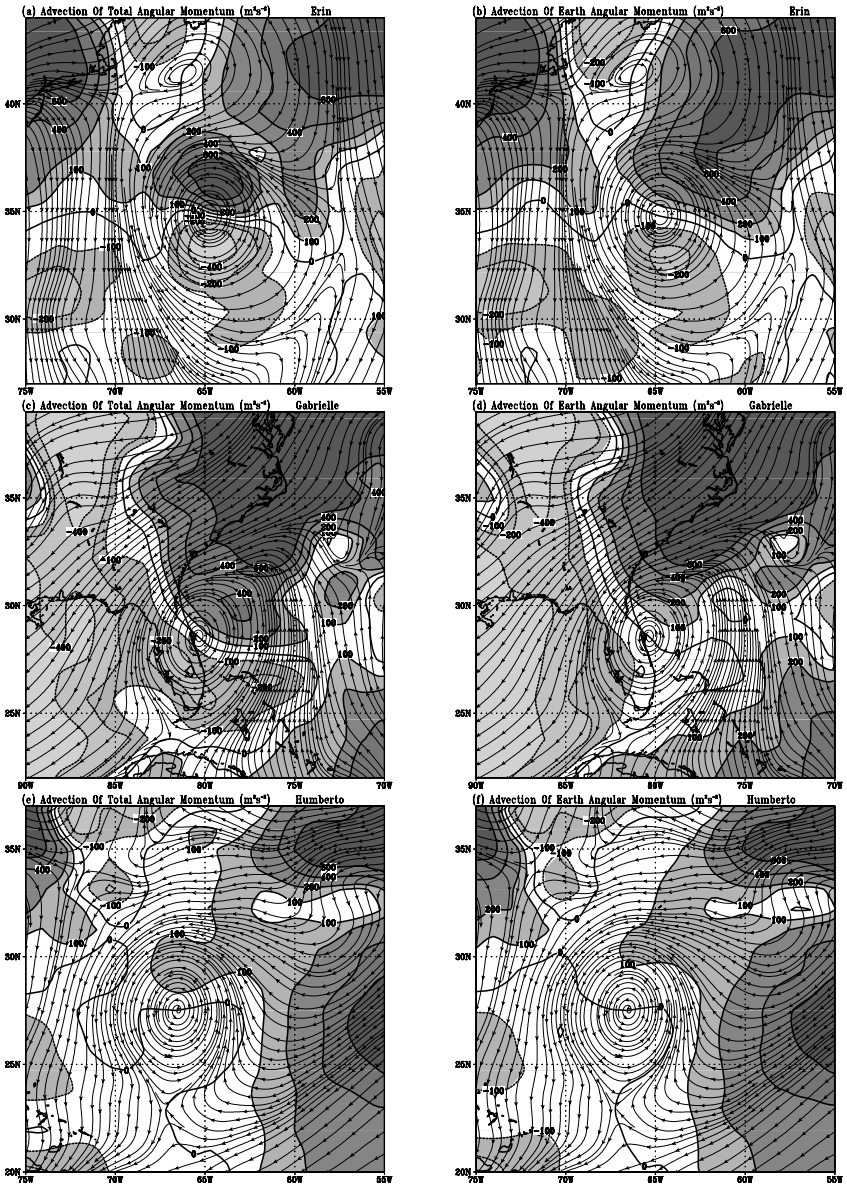

Fig 17. Storm-relative advection (at the 850-hPa level) of total angular momentum (left panels) and of Earth angular momentum (right panels) for hurricanes Erin (top panels), Gabrielle (middle panels) and Humberto (bottom panels). Units are m^2 s^{-2}. The storm-relative streamlines at 850 hPa are superimposed. Shaded regions correspond to values greater than 100 units.

momentum (right panels of Fig. 17). In Erin and Humberto we do not see a grand sweep of negative advection of total and Earth angular momentum from the north-west and into the storm center. These storms maintained their hurricane intensity for several days subsequent to this picture. Hurricane Gabrielle did exhibit the intrusion of negative total angular momentum from the west and north-west of the storm. Close to the storm center, positive values of Earth angular momentum were found. What seems different in Lili compared to these other hurricanes is that a large negative value for advection of Earth's angular momentum such as -100 to -400 m^2 s^{-2}, near the center of the storm, were only seen for Lili. The superimposed streamlines in all these panels show storm-relative flow field at the 850-hPa level.

6. Conclusions

An important scientific question asked recently at a hurricane conference was on the reason for the sudden demise of Hurricane Lili. On the face of it, two propositions are frequently made. One is the dry air incursion as was noted in the water vapor imagery. The second factor was the cooler SSTs that were noted in the northern Gulf of Mexico in the wake of Hurricane Isidore that preceded Lili. Cooler than normal SSTs were also noted in the eastern parts of the Gulf of Mexico. The temperatures over most of the Gulf of Mexico were, in fact, not quite that cold, as the anomalies over most regions were within 1°C to 1.5°C in the area where the hurricane traversed. This paper exploits a new

technique called 'with and with' partitioning of a model run, where it is possible to accumulate the contributions to the surface pressure tendencies arising from different components of the model's dynamics and physics. Following this rationale, it was possible to suppress the effects of dry air advection into the storm and obtain its contributions to the pressure rise, when in fact all other features of the model were retained. Several experiments failed to show any significant impact on Hurricane Lili's pressure tendency from these partitioning exercises. Overall, this pressure rise was only a few hPa in 36 h of forecast, far short of the noted pressure rise of 23 hPa in 13 h. An exercise on the residue free budget from the contributions of the evaporative fluxes from the ocean also demonstrated small contributions of the order of a few hPa to the pressure rise issue. The cold anomaly of about a degree (°C) did not seem to suppress the evaporative fluxes sufficiently to affect the storm intensity in any marked manner. The impact of surface moisture fluxes was also explored using the 'with and without' strategy. A straight 36-h forecast, where the humidity flux was removed entirely, showed that the effect of humidity flux could have a large impact, i.e. 20 hPa 36 h^{-1} of pressure rise. We discounted these results because these did not permit the co-evolution of dynamics and physics. Noting that the 'with and with' strategy provides a more correct answer to these questions, we conclude that suppressed air–sea interaction due to the presence of cooler SSTs over the northern Gulf was not an important factor in the demise of Lili.

Our full model run did capture a pressure rise of 22 hPa in 36 h that was close to the observed pressure rise. This was accomplished by deliberately making six six-hourly forecasts sequentially with restarts using real data and physical initialization. The purpose of this was to reduce forecast errors and to generate a data set that could be diagnosed using the proposed 'with and with' strategy. This procedure worked where a straight 36-h forecast failed to predict the pressure rise accurately. The 'with and with' strategy provided a different insight on the reasons for the weakening of Hurricane Lili from a category 4 to a category 1 storm in its last 13 h prior to landfall. The advective dynamics appeared to contribute to a net drop in pressure, i.e. calling for a further deepening of Lili in these last 13 h. The advective dynamics included the effects of advection of vorticity, divergence, and temperature in the system of equations. Among these, the advection of vorticity was the more important contribution. This did include the horizontal as well as the vertical advective components. These two terms tend to cancel each other somewhat; however, there was a net residual that contributed to a drop of pressure for Hurricane Lili. This drop in pressure was offset by a substantial pressure rise from the 'rest of dynamics' of the entire system of equations.

This component of the model turned out to be the most important contributor for the demise of Lili. The largest contributor in the 'rest of dynamics' came from the vorticity equation. To answer the question about how the 'rest of dynamics' contributes to a pressure rise in Lili, we examined the equivalent of this term from the angular momentum dynamics. The Coriolis-divergence term of the vorticity equation is equivalent to the Earth's angular momentum terms in the angular momentum equation. In this context, the transport of Earth angular momentum in storm-relative coordinates, $(\mathbf{V} - \mathbf{C}) \cdot \nabla \mathbf{fr}^2/2$ was the most important contributor. The field of advection of Earth angular momentum (equivalent to our 'rest of dynamics') carried a pronounced field of negative angular momentum transported from the north-west of Lili to its center. This transport field, in storm-relative coordinates, is expected to last for several hours (moving with the storm). This large negative advection of Earth angular momentum contributes to a loss of spin of the storm and leads to its weakening. The horizontal and vertical advection of relative angular momentum balance each other somewhat closely; this is similar to the close balance among the horizontal and vertical advection of momentum in large-scale dynamics. The same is not true for the Earth's angular momentum; its horizontal advection can be substantial whereas its vertical advection is always zero, because $(\partial/\partial\sigma)\,(\mathbf{fr}^2/2) = 0$. In that sense, the horizontal advection of the Earth's angular momentum has a special significance. As the spin is reduced, the pressure adjusts to it and the warm core weakens towards a weaker hydrostatic thickness. This entire sequence of events can, in principle, be mapped. This belt of negative advection of angular momentum that enters the storm center is very similar to the geometry of the dry air incursion from the north-west that was seen in the water vapor imagery from the geostationary satellite. Our conclusion is that between these two similar features the weakening of Lili followed the incursion of negative Earth angular momentum and not as much from that of the dry air. The physical processes contributed to a net pressure drop with the largest contribution arising from the parametrization of deep cumulus convection. These effects had a negative impact on the observed pressure rise of Lili. In the thermodynamic equation, we note a role of shallow moist convection eroding the warm core by a net cooling of the temperature tendencies and for the overall pressure rise of Hurricane Lili.

We have looked at the fields of the relative angular momentum transports for Lili (a weakening storm) and several mature hurricanes. Based on these, we feel that a regular monitoring of such dynamical fields that relate to the spin of a hurricane may be important. The entire issue of angular momentum and the intensity of hurricanes deserves a much more careful study. This will be a subject of a separate paper. What we see here is that as parcels move inwards from the outer radii of the hurricane, the relative angular momentum increased, the Earth angular momentum decreased, a loss of angular momentum also occurred from the surface and cloud scale frictional torques. The final intensity of Lili was determined from an intricate balance among these components. The present study points to the important role of the Earth's angular momentum, and its changes, in storm-relative coordinates. This happened to fall under the category of 'rest of dynamics' in our partitioning of the model pressure tendencies.

7. Acknowledgements

The work presented in this paper was supported by the following grants: NSF Grant ATM-0108741, NASA Grant NAG8-1848, NASA Grant NAG5-9662 and FSU Research Foundation Award No. 1338-745-45.

8. Appendix A: Outline of the FSU Global Spectral Model

The salient features of the high-resolution FSU global spectral model used in this study are as follows.

(1) Horizontal resolution T255.

(2) Vertical resolution 14 layers between the surface and 50-hPa level.

(3) Semi-implicit time differencing.

(4) Spectral transform method for non-linear dynamics.

(5) Fourth-order horizontal diffusion (Kanamitsu et al., 1983).

(6) Shallow moist convection following Tiedtke (1984).

(7) Dry convective adjustment.

(8) Deep convection following Krishnamurti and Bedi (1988).

(9) Classical radiative transfer based on emissivity/absorptivity for long and short wave radiative fluxes following Chang (1979).

(10) Surface energy balance for providing diurnal change (Krishnamurti et al., 1991b).

(11) Envelope orography following Wallace et al. (1983).

(12) Surface fluxes based on surface similarity theory (Businger et al., 1971). Planetary boundary layer fluxes based on K theory where the diffusion coefficients are determined from a mixing length and Richardson number dependence (Louis, 1979).

References

Businger, J. A., Wyngard, J. C., Izumi, Y. and Bradley, E. F. 1971. Flux profile relationship in the atmospheric surface layer. *J. Atmos. Sci.* **28**, 181–189.

Chang, C. B. 1979. On the influence of solar radiation and diurnal variation of surface temperatures on African disturbances. *Report 79-3*, Department of Meteorology, Florida State University, 157 pp.

Kamineni, R., Krishnamurti, T. N., Ferrare, R. A., Ismail, S. and Browell, E. V. 2003. Impact of high-resolution water vapor cross-sectional data on hurricane forecasting. *Geophy. Res. Lett.* **30**(5), 1234.

Kanamitsu, M., Tada, K., Kudo, K., Sato, N. and Ita, S. 1983. Description of the JMA operational spectral model. *J. Meteorol. Soc. Japan* **61**, 812–828.

Krishnamurti, T. N. and Bedi, H. S. 1988. Cumulus parametrization and rainfall rates III. *Mon. Wea. Rev.* **116**, 583–599.

Krishnamurti, T. N., Oosterhof, D. K. and Dignon, N. 1989. Hurricane prediction with a high resolution global model. *Mon. Wea. Rev.* **117**, 631–669.

Krishnamurti, T. N., Xue, J., Bedi, H. S., Ingles, K. and Oosterhof, D. 1991a. Physical initialization for numerical weather prediction over the tropics. *Tellus* **43AB**, 53–81.

Krishnamurti, T. N., Yap, K. S. and Oosterhof, D. K. 1991b. Sensitivity of tropical storm forecast to radiative destabilization. *Mon. Wea. Rev.* **119**, 2176–2205.

Krishnamurti, T. N., Bedi, H. S., Yap, K. S. and Oosterhof, D. 1993. Hurricane forecasts in the FSU models. *Adv. Atmos. Sci.* **10**, 121–132.

Krishnamurti, T. N., Rohaly, G. and Bedi, H. S. 1994. On the improvement of precipitation forecast skill from physical initialization. *Tellus* **46A**, 598–614.

Krishnamurti, T. N., Bedi, H. S., Rohaly, G. D. and Oosterhof, D. 1996. Partitioning of the seasonal simulation of a monsoon climate. *Mon. Wea. Rev.* **124**, 1499–1519.

Krishnamurti, T. N., Bedi, H. S. and Hardiker, V. M. 1998. *An Introduction to Global Spectral Modeling*. Oxford University Press, Oxford, 253 pp.

Krishnamurti, T. N., Surendran, S., Shin, D. W., Correa-Torres, R. J., Vijaya Kumar, T. S. V. et al. 2001. Real-time multianalysis-multimodel superensemble forecasts of precipitation using TRMM and SSM/I products. *Mon. Wea. Rev.* **129**, 2861–2883.

Krishnamurti, T. N., Sanjay, J., Mitra, A. K. and Vijaya Kumar, T. S. V. 2004. Forecast errors arising from different components of a model physics and dynamics. *Mon. Wea. Rev.* **132**, in press.

Louis, J. F. 1979. A parametric model of vertical eddy fluxes in the atmosphere. *Bound.-Layer Meteor.* **17**, 187–202.

O'Shay, A. and Krishnamurti, T. N. 2004. An examination of a model' components during tropical cyclone recurvature. *Mon. Wea. Rev.* **132**, 1143–1166.

Pasch, R. J., Lawrence, M. B., Avila, L. A., Beven, J. L., Franklin, J. L. and Stewart, S. R. 2004. Atlantic Hurricane Season of 2002. *Mon. Wea. Rev.* **132**, 1829–1859.

Shay, L., Cook, T., Mainelli, M., Evans, R., White, S. et al. 2003. Improving hurricane heat potential estimates: effects of daily sea surface temperatures. In: Proc. 57th Interdepartmental Hurricane Conference, March 10–14, Miami, FL. Available online from the web site http://www.ofcm.gov/ihc03/presentations/03-session3_recon_and_obs/03_shay.ppt

Thu, T. V. and Krishnamurti, T. N. 1992. Vortex initialization for typhoon track prediction. *J. Meteorol. Atmos. Phys.* **47**, 117–126.

Tiedtke, M. 1984. The sensitivity of the time-mean large-scale flow to cumulus convection in the ECMWF model. In: Proc. Workshop on Convection in Large-Scale Numerical Models. ECMWF, Reading, UK, 297–316.

Wallace, J. M., Tibaldi, S. and Simmons, A. J. 1983. Reduction of systematic forecast errors in the ECMWF model through the introduction of envelope orography. *Q. J. R. Meteorol. Soc.* **109**, 683–718.

Williamson, D. L. 2002. Time-split versus process-split coupling of parametrizations and dynamical core. *Mon. Wea. Rev.* **130**, 2024–2041.